Transient temperature phenomena during sublimation growth of silicon carbide single crystals*

Olaf Klein and Peter Philip

July 18, 2002

Abstract

In this article, we use numerical simulation to investigate transient temperature phenomena during sublimation growth of SiC single crytals via physical vapor transport (also called the modified Lely method). We consider the evolution of temperatures at the SiC source and at the SiC seed crystal, which are highly relevant to the quality of the grown crystals, but inaccessible to direct measurements. The simulations are based on a transient mathematical model for the heat transport, including heat conduction, radiation, and radio frequency (RF) induction heating. Varying the position of the induction coil as well as the heating power, it is shown that the measurable temperature difference between the bottom and the top of the growth apparatus can usually not be used as a simple indicator for the respective temperature difference between SiC source and seed. Moreover, it is shown that there can be a time lack of 1.5 hours between the heating of the temperature measuring points and the heating of the interior of the SiC source.

2000 Mathematics Subject Classification: 80A20, 65C20, 65Z05.

1998 PACS numbers: 81.10.Bk, 44.05.+e, 02.60.Cb.

Keywords and Phrases: Temperature evolution. Heating stage. Sublimation growth. Physical vapor transport. Modified Lely method. SiC single crystal. SiC powder source. Temperature difference. Transient modeling. Numerical simulation.

1 Introduction

Due to its advantageous physical properties, silicon carbide (SiC) is used in numerous industrial applications. As a semiconductor substrate material, SiC is utilized in

*This work has been supported by the DFG Research Center "Mathematics for key technologies" (FZT 86) in Berlin and by the German Federal Ministry for Education and Research (BMBF) within the program "Neue Mathematische Verfahren in Industrie und Dienstleistungen" ("New Mathematical Methods in Manufacturing and Service Industry") # 03SPM3B5.

electronic and optoelectronic devices such as MESFETs, MOSFETs, thyristors, P-i-N diodes, Schottky diodes, blue and green LEDs, lasers, and sensors. Its chemical and thermal stability enable SiC to be used in high temperature applications as well as in intensive radiation environments. Moreover, SiC is especially suitable for usage in high power and high frequency applications.

An economically profitable use of SiC requires the availability of low-defect SiC boules with large diameter. Moreover, a high growth rate during the production process is desirable to reduce production time and cost. Even though there has been substantial progress in SiC manufacturing in recent years, satisfying all of the aforementioned demands remains challenging, as only partial solutions exist (cf. e.g. [GHTC97], [CTG+99], [MGH+01]).

We consider the production of SiC single crystals by sublimation growth via *physical vapor transport* (PVT) (modified Lely method, see e.g. [Kon95]). Typically, modern PVT growth systems consist of an induction-heated graphite crucible containing polycrystalline SiC source powder and a single-crystalline SiC seed (cf. Fig. 1). The source powder is placed in the hot zone of the growth apparatus, whereas the seed crystal is cooled by means of a blind hole, establishing a temperature difference between source and seed.

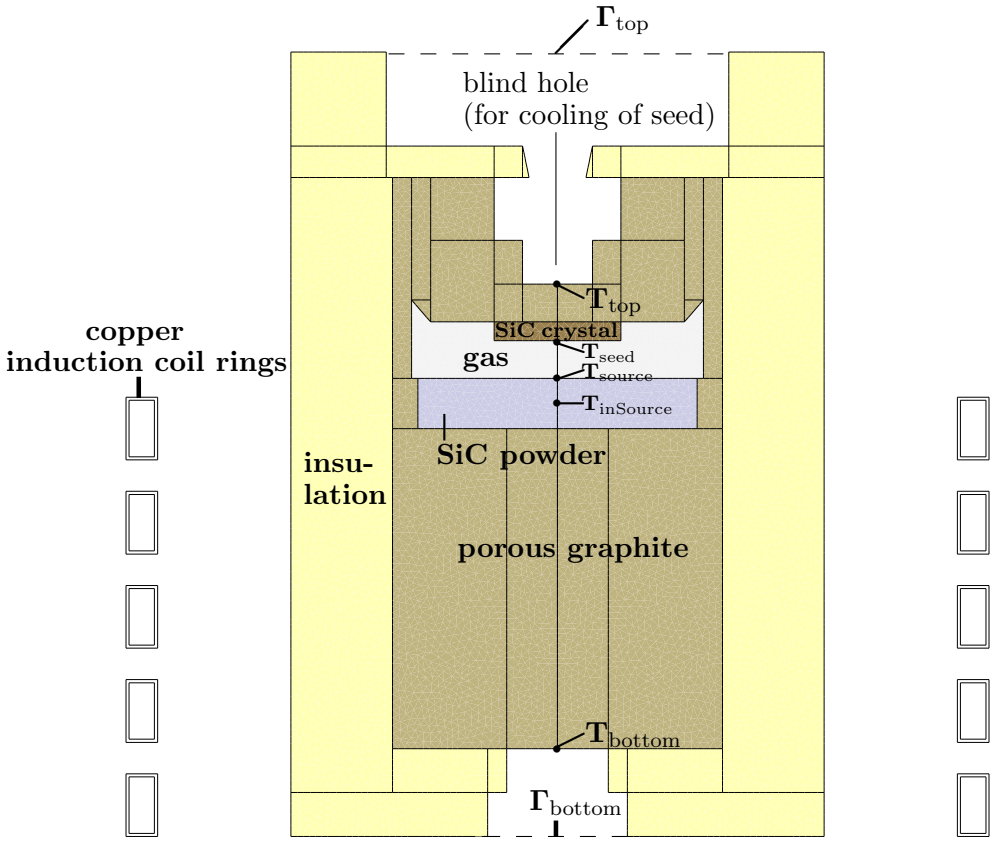

Figure 1: Setup of growth apparatus according to [PAC+99, Fig. 2].

To eliminate contaminants such as S, B, and metallic elements from the growth

system, in a first heating stage, the apparatus is degassed at some 10^{-3} Pa and heated to about 1200 K. After the contaminant bakeout phase has been completed, a high-purity argon atmosphere is established at 10^5 Pa, and the temperature is further increased. At growth temperature, which can reach up to 3000 K for growth of the SiC polytype 6H, pressure is reduced to about $2 \cdot 10^3$ Pa (cf. [BMH+93]).

After growth temperature has been reached, the SiC source is kept at a higher temperature than the cooled SiC seed, such that sublimation is encouraged at the source and crystallization is encouraged at the seed, causing the partial pressures of Si, Si_2C and SiC_2 to be higher in the neighborhood of the source and lower in the neighborhood of the seed. As the system tries to equalize the partial pressures, source material is transported to the seed which grows into the reaction chamber.

It is found (cf. e.g. [SBP98], [RSD+99], and [SVK+00]) that the crystal's defect density and growth rate are strongly influenced by the temperature distribution (especially the temperature at the seed and the temperature difference between source and seed), the mass transport, and the pressure and concentrations of gas species. These *internal control parameters* can only be tuned indirectly by varying *external control parameters* such as the geometrical configuration of the setup, the power of the RF heater, the position of the induction coil, and the inert gas pressure.

Due to the high temperatures, experimental verification of the correlation between the properties of the grown crystal and both internal and external control parameters is very intricate and costly. Hence, theoretical modeling and numerical simulation play an essential role in the investigation and determination of the relation between controllable quantities and advantageous growth conditions. In consequence, the development of numerical models and software and their application to PVT growth of SiC crystals has been an active field of research in recent years. Recent papers on stationary models include [PAC+99], [KKZ+00], [SKM+00]. Transient models are considered in [Råb96], [CZP01], [CZP+99], [KPSW01], [KP01], [DCK+02], where the last four papers discuss transient numerical results concerning the heat transfer during PVT.

It is not sufficient to restrict one's attention to the quasi-stationary state at the end of the heating process, but it is also important to monitor and control the temperature field evolution during the heating process itself: Crystal growth can already occur during the heating-up stage, possibly causing micropipes or the growth of unwanted polytypes. Moreover, thermal stresses in the seed crystal due to temperature gradients during heating can initiate crystal defects. Finally, the transient numerical simulations presented in this article show a significant time lack between the heating of the interior of the SiC source and the bulk of the apparatus. We investigate the dependence of the time lack on the amount of used source powder and on the powder's thermal conductivity. The results can help to gauge the time one has to allow for the contaminant bakeout phase described above.

Moreover, we investigate how the measurable temperature difference between the lower and the upper blind hole is related to the growth-controlling temperature difference between source and seed. It is shown that, in general, there is no simple

relation between both differences. For the considered growth configuration, the relation depends critically on the position of the induction coil and on the heating power.

2 Modeling of Heat Transfer and Induction Heating

To obtain the numerical results of Sec. 3 below, we have employed our transient model of heat transport in induction-heated PVT growth systems, previously described in [BKP+99], [KPSW01], [KP01], and [KP02]. It is assumed that all components of the growth system as well as all relevant physical quantities are cylindrically symmetric. The heat transport model includes conduction through solid materials as well as through the gas phase. Radiative heat transfer between surfaces of cavities is included using the net radiation method for diffuse-gray radiation as described in [KPSW01]. All solids are treated as opaque, except the SiC single crystal, where semi-transparency is accounted for via the band approximation model. It is assumed that the growth apparatus is exposed to a black body environment (e.g. a large isothermal room) radiating at room temperature T_{room}, such that outer boundaries emit according to the Stefan-Boltzmann law. For the two blind holes, we use black body phantom closures (denoted by Γ_{top} and Γ_{bottom} in Fig. 1) which emit radiation at T_{room}. Thus, we allow for radiative interactions between the open cavities and the ambient environment, including reflections at the cavity surfaces. The view factor algorithm is based on [DNR+90] and is described in [KPSW01, Sec. 4].

Induction heating causes eddy currents in the conducting materials of the growth apparatus, resulting in heat sources due to the Joule effect. Assuming sinusoidal time dependence of the imposed alternating voltage, the heat sources are computed via an axisymmetric complex-valued magnetic scalar potential that is determined as the solution of an elliptic partial differential equation (s. [KP01, Sec. 2]). To prescribe the total heating power, we use the method described in [KP02, Sec. II], assuring that the total current is the same in each coil ring. The distribution of the heat sources is redetermined in each time step of the transient problem for the temperature evolution to account for temperature dependence of the electrical conductivity.

A finite volume method is used for the discretizations arising in the stationary computation of the magnetic scalar potential and in the transient temperature simulations. An implicit Euler scheme provides the time discretization of the temperature evolution equation; only emissivity terms are evaluated explicitly, i.e. using the temperature at the previous time step. The nonlinear systems arising from the finite volume discretization of the nonlinear heat transport problem are solved by Newton's method.

All simulations were performed using the software *WIAS-HiTNIHS*[1] which is based on the program package *pdelib* being developed at the *Weierstrass Institute of Applied Analysis and Stochastics (WIAS)*, Berlin (cf. [FKL01]).

3 Numerical Results and Discussion

3.1 General Setting

All numerical simulations presented in the following were performed for the growth system [PAC+99, Fig. 2] displayed in Fig. 1, consisting of a container having a radius of 8.4 cm and a height of 25 cm placed inside of 5 hollow rectangular-shaped copper induction rings. The geometric proportions of the coil rings are provided in Fig. 2.

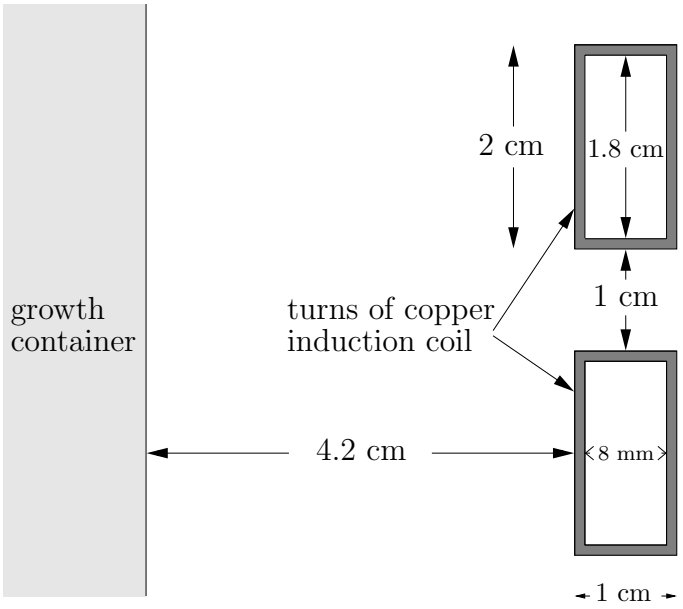

Figure 2: Geometric proportions of induction coil rings.

Usually, during a physical growth run, the SiC source powder graphitizes and sinters, and chemical reactions inside the solid parts of the graphite crucible lead to changes in its porosity and can cause nonsealing joints. Moreover, accumulation of Si in the insulation felt is observed. It is not feasible to account for these changes at the current stage of numerical simulations. Hence, all simulations presented in this article are performed for an idealized growth apparatus, treating all solid materials as homogeneous and pure. Except for the thermal conductivity of the SiC source

[1] **Hi**gh **T**emperature **N**umerical **I**nduction **H**eating **S**imulator; pronounciation: ∼nice.

powder provided in Appendix A, the material data used for the following numerical experiments are precisely the data provided in the appendices of [KPSW01] and [KP01], respectively.

As described in [KPSW01, Sec. 5], for simulations of the temperature distribution evolution, it is reasonable to assume that the gas phase is made up solely of argon, notwithstanding the fact that species such as Si, Si_2C, and SiC_2 make up a significant portion of the gas mixture at high temperatures.

The angular frequency used for the induction heating is $\omega = 2\pi f$, where $f = 10$ kHz. The average total power P is prescribed according to the following linear ramp:

$$P(t) := \begin{cases} \frac{P_{\max}}{t_{\text{ramp}}} \cdot t & \text{for } 0 \le t \le t_{\text{ramp}}, \\ P_{\max} & \text{for } t \ge t_{\text{ramp}}, \end{cases} \tag{3.1}$$

where $t_{\text{ramp}} = 2$ h. Moreover, $P_{\max} = 7$ kW, except for the experiments depicted in Fig. 4.

Each simulation starts at $T_{\text{room}} = 293$ K, computing and monitoring the evolution of the temperature distribution in the growth apparatus.

3.2 Temperature Differences

In a series of five numerical experiments, we investigate the relation between the temperature differences $T_{\text{bt}} := T_{\text{bottom}} - T_{\text{top}}$ and $T_{\text{ss}} := T_{\text{source}} - T_{\text{seed}}$ (cf. Fig. 1) for three different coil positions and, for the lowest coil position, for three different values of $P_{\max}$ (cf. (3.1)). The relation is of importance, as in physical growth experiments, T_{bottom} and T_{top} are measured, and T_{bt} is often used as an indicator for T_{ss} which is not accessible to direct measurements, but crucial for the growth process.

For the three simulations using $P_{\max} = 7$ kW, the results for the respective evolutions of T_{bt} and T_{ss} are depicted in Fig. 3. In Fig. 3(a), the coil is in the highest position, between vertical coordinates $z = 4$ and $z = 18$ cm, in Fig. 3(b), the coil is in medium position, between $z = 2$ cm and $z = 16$ cm, and in Fig. 3(c), the coil is in the lowest position, between $z = 0$ cm and $z = 14$ cm.

Figure 3 shows that the evolution of T_{ss} is almost independent of the chosen coil position, whereas the behavior of T_{bt} changes drastically with the coil position. In all three cases, T_{bt} is no indicator for T_{ss} before T_{ss} has reached its quasi-stationary final state, but, more importantly, even in the stationary state at growth temperature, T_{ss} and T_{bt} are of comparable magnitude only for the lowest coil position. In Figures 3(a) and 3(b), not even the signs of T_{ss} and T_{bt} agree in the final state.

Moreover, the good agreement of T_{ss} and T_{bt} in the final state of Fig. 3(c) is merely coincidental in the sense that the agreement is lost for other values of $P_{\max}$. For the same coil position as in Fig. 3(c), Fig. 4 shows that T_{bt} is almost three times as large as T_{ss} in the final state if $P_{\max}$ is reduced to 5.5 kW (Fig. 4(a)), and that T_{bt} and T_{ss} have different signs if $P_{\max}$ is increased to 8.5 kW (Fig. 4(b)).

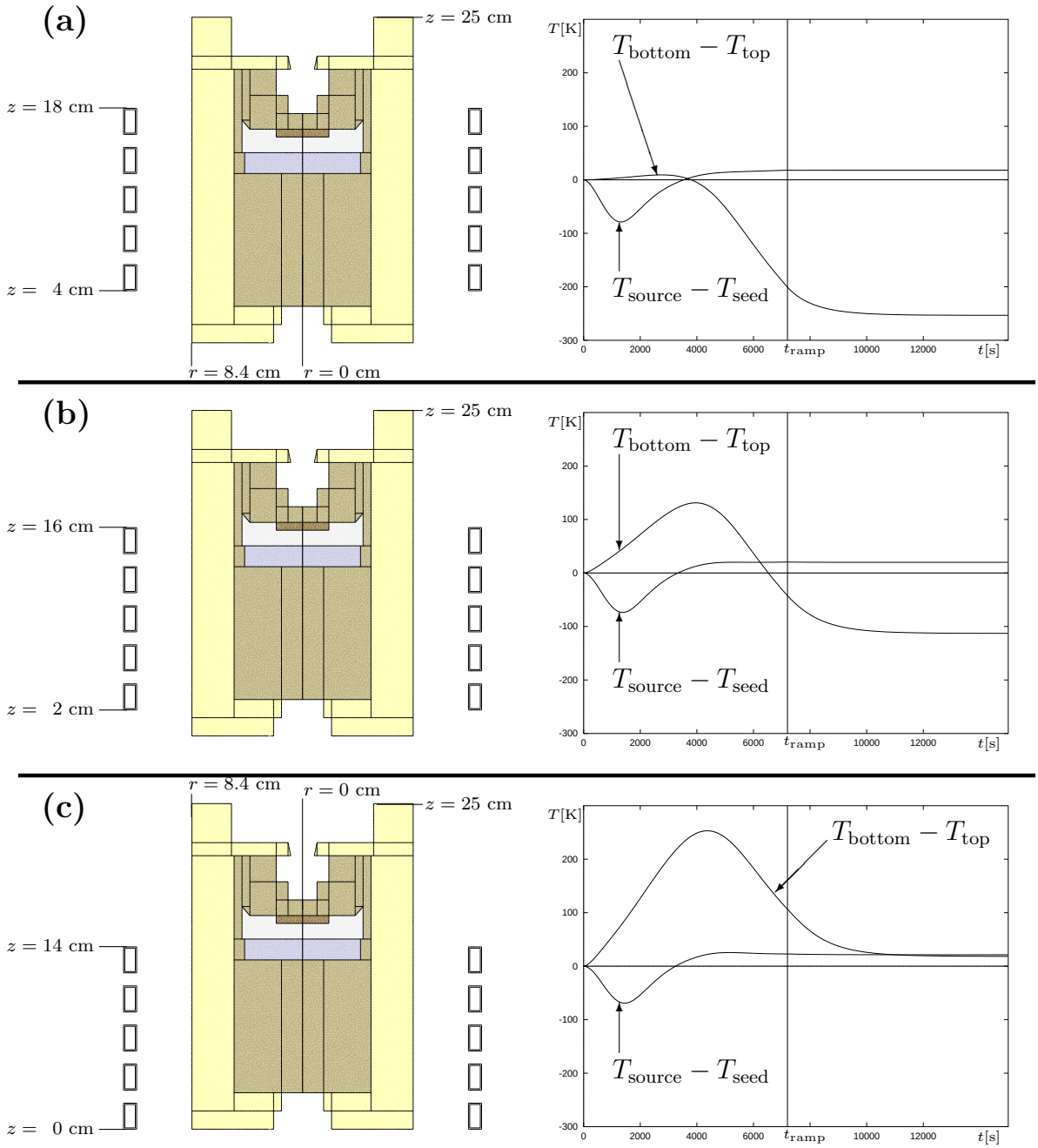

Figure 3: The evolution of the temperature differences $T_{\text{bottom}} - T_{\text{top}}$ and $T_{\text{source}} - T_{\text{seed}}$ is compared for three different positions of the induction coil. The respective positions of the induction coil are given by the specifications on the left-hand side. For the respective locations of T_{bottom}, T_{top}, T_{source}, and T_{seed}, it is referred to Fig. 1. The heating power is increased linearly according to (3.1) with $P_{\max} = 7$ kW.

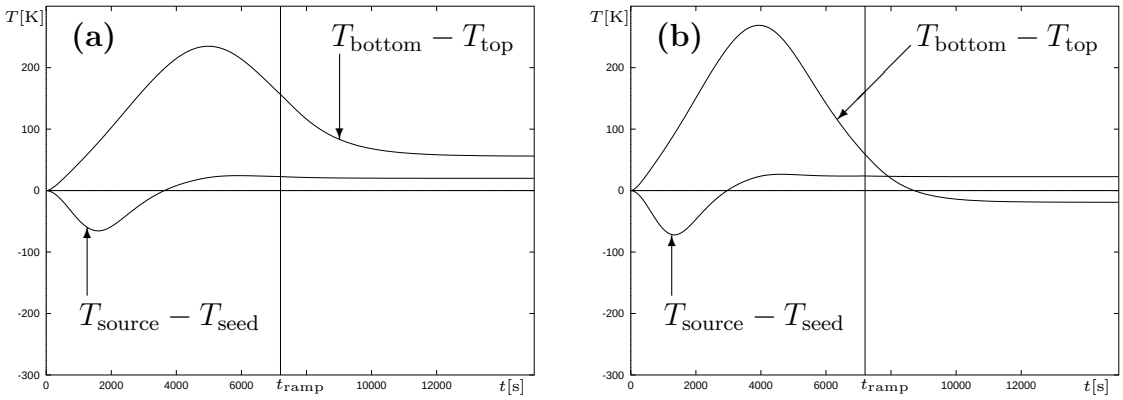

Figure 4: As in Fig. 3(a), the evolution of the temperature differences $T_{\text{bottom}} - T_{\text{top}}$ and $T_{\text{source}} - T_{\text{seed}}$ is depicted for a numerical experiment using the lowest coil position. In contrast to Fig. 3(a), the power $P_{\max}$ in (3.1) is set to 5.5 kW in Fig. 4(a) and to 8.5 kW in Fig. 4(b).

The numerical experiments show that for the considered configuration, there is generally no easy relation between T_{ss} and T_{bt}. Even though there might be configurations where the situation is better, for each real growth system, the validity of using T_{bt} as an indicator for T_{ss} needs to be verified by some other method (e.g. numerical simulation).

3.3 Heating of SiC Source Powder

In a series of five numerical experiments, we investigate the evolution of the temperature at the center of the SiC powder source in comparison with the temperature evolutions of T_{top}, T_{bottom}, and T_{source} (cf. Fig. 1) for three different quantities of the powder charge and, for the largest powder quantity, for three different laws for the thermal conductivity of the SiC powder. In comparison with the experiment depicted in Fig. 5(a), the amount of SiC powder is tripled in the experiment depicted in Fig. 5(b), and in the experiment depicted in Fig. 5(c), it is fivefold the original amount. For the numerical experiments considered in Fig. 5, we use (A.1) of Appendix A for the thermal conductivity of the SiC powder. The same law was used in Sec. 3.2. The law is multiplied by 3 and 5, respectively, for the simulations studied in Fig. 6.

The low coil position of Fig. 3(c) was used for all simulations considered in the following. However, we note that we found similar results for the higher coil positions used in Figures 3(a) and 3(b).

Figure 5 shows that for the considered configuration and if the thermal conductivity of the powder charge behaves according to (A.1), then there is a considerable time lack between the heating of the bulk of the apparatus and the heating of the inte-

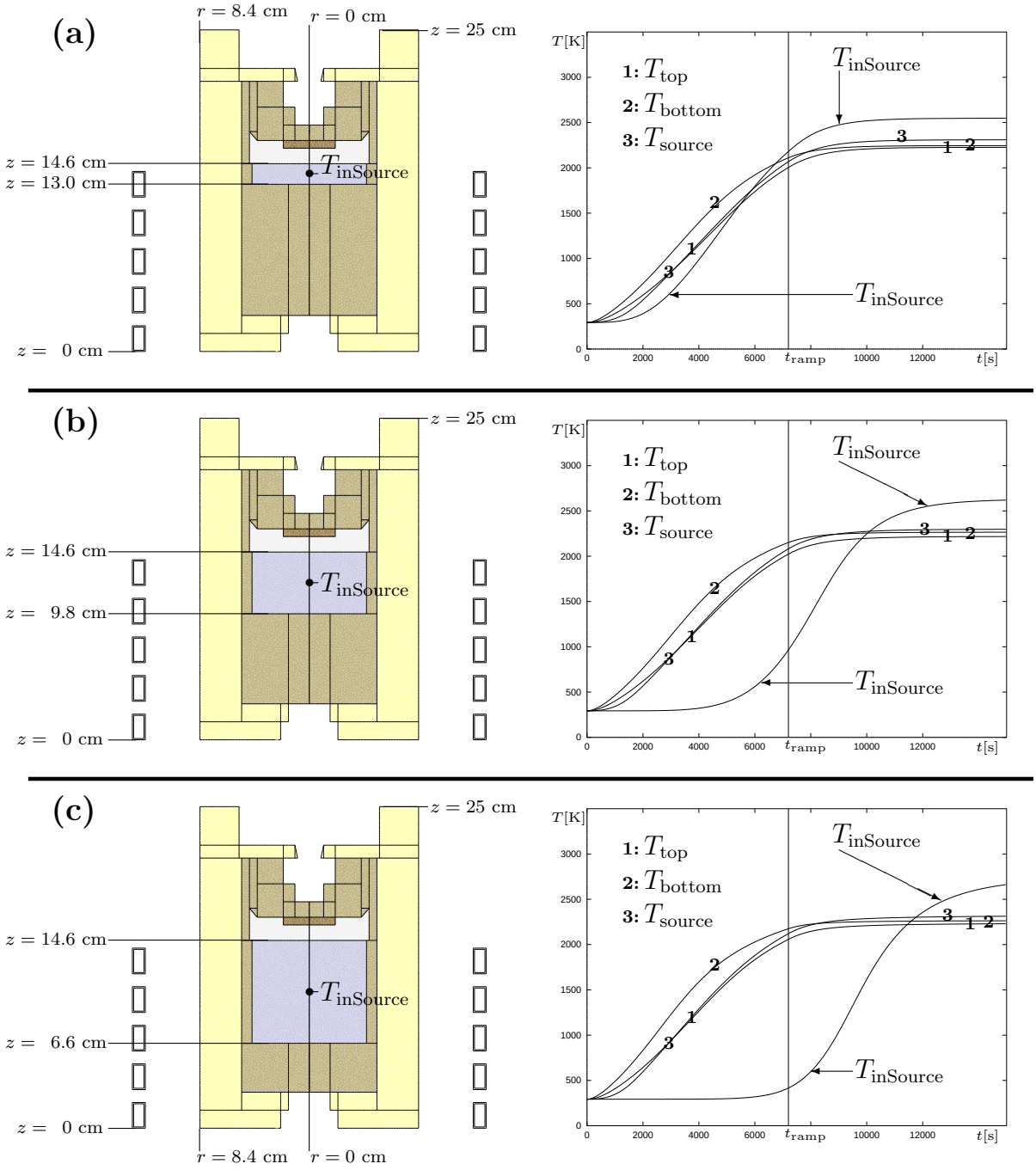

Figure 5: The evolution of T_{inSource} is compared to the evolutions of T_{top}, T_{bottom}, and T_{source} for three different amounts of the powder charge. In comparison with (a), the amount of the powder is tripled in (b) and 5-fold in (c). For the respective locations of T_{top}, T_{bottom}, and T_{source}, confer Fig. 1. The heating power is increased linearly according to (3.1) with $P_{\max} = 7$ kW.

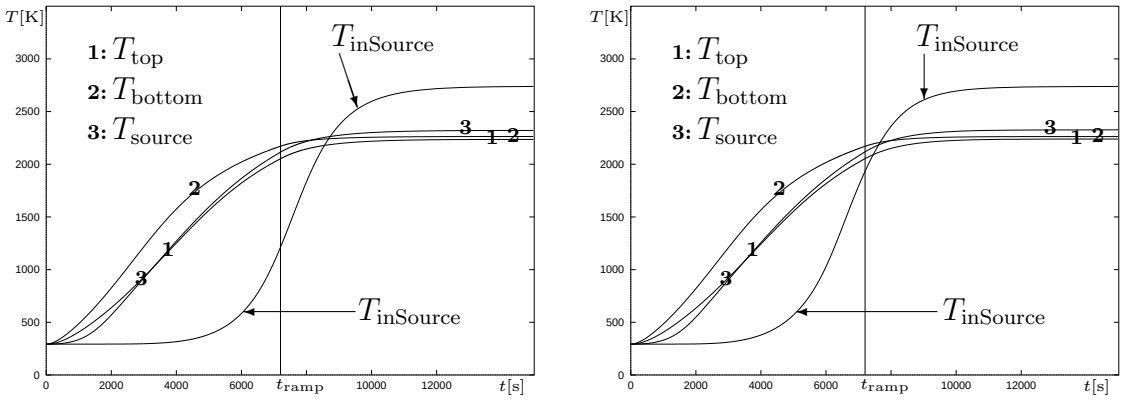

Figure 6: As in Fig. 5(c), the evolution of T_{inSource} is compared to the evolutions of T_{top}, T_{bottom}, and T_{source} for the largest powder charge. In comparison with the experiments depicted in Fig. 5, the thermal conductivity of the SiC powder has been multiplied by 3 in Fig. 6(a) and by 5 in Fig. 6(b).

rior of the SiC powder charge. Whereas the evolution of T_{top}, T_{bottom}, and T_{source}, respectively, is almost independent of the considered powder quantities, the heating of the powder's center is increasingly delayed in Figures 5(b) and 5(c).

Since the physical properties of used powder charges vary considerably, we performed two simulations for the configuration of Fig. 5(c), i.e. with the largest amount of SiC powder, where the powder's thermal conductivity is multiplied by 3 and 5, respectively, in comparison with the simulations considered in Fig. 5. The results are depicted in Fig. 6. As expected, the higher thermal conductivity speeds up the heating of the powder's center, but in both cases it is still considerably delayed with respect to the bulk of the apparatus (also cf. Table 1).

As described in the Introduction, the growth system is usually kept at some 1200 K and at low pressure for a certain time, to bake out contaminants from the source powder. For the experiments where the thermal conductivity of the powder charge is set according to (A.1), Table 1 shows that while the time lack between T_{top} reaching 1200 K and T_{inSource} reaching 1200 K is merely 5 minutes for the smallest powder charge, it increases to 1 hour for the medium powder charge and to 1.5 hours for the largest powder charge. For the largest powder charge, the time lack is still 39 minutes, even if its thermal conductivity is multiplied by 5. Thus, depending on the configuration of the growth system, it can be of paramount importance to take into account this time lack, in order to allow sufficient time for the contaminant bake-out phase.

The time lack between the heating of the powder's surface and its interior has been independently studied in [DCK$^+$02], where its significance with respect to graphitization of the powder source is investigated.

	$t_1 := t(T_{\text{top}} = 1200\ \text{K})$ [min]	$t_2 := t(T_{\text{inSource}} = 1200\ \text{K})$ [min]	$(t_2 - t_1)$ [min]
Fig. 5(a)	70	75	5
Fig. 5(b)	66	128	62
Fig. 5(c)	63	155	92
Fig. 6(a)	64	120	56
Fig. 6(b)	65	104	39

Table 1: Time lack between T_{top} reaching 1200 K and T_{inSource} reaching 1200 K for the five numerical experiments considered in Figures 5 and 6, respectively.

4 Conclusions

Using transient numerical simulation of the temperature evolution of the heating process of PVT growth systems, it was shown that for the configuration of Fig. 1, there is no simple relation between the directly measurable temperature difference between the lower blind hole and the upper blind hole and the temperature difference between SiC source and SiC seed. The relation depends strongly on the coil position and the heating power, and often the two differences do not even have the same sign.

Moreover, it was found that the heating of the SiC source powder can be significantly delayed in comparison with the heating of the bulk of the growth apparatus. As one expects, this effect becomes more prominent if a larger powder charge is used, and it becomes less prominent if the powder has a higher thermal conductivity. For the considered configuration, we found a time lack of up to 1.5 hours between the heating of the powder surface and its interior. It is thus necessary to take this expected time lack into account when designing growth experiments, e.g. to allow sufficient time for the contaminant bake-out phase.

Acknowledgments

We thank Jürgen Sprekels of the WIAS Berlin as well as Klaus Böttcher, Detlev Schulz, and Dietmar Siche of the Institute for Crystal Growth, Berlin, for helpful discussions and advice. We gratefully acknowledge financial support by the *Bundesministerium für Bildung, Wissenschaft, Forschung und Technologie*[2] *(BMBF)* within the program *Neue Mathematische Verfahren in Industrie und Dienstleistungen*[3] # 03SPM3B5.

[2]German Ministry for Education, Science, Research, and Technology

[3]New Mathematical Methods in Manufacturing and Service Industry

A Appendix: Thermal Conductivity in SiC Source Powder

The material data used for the simulations presented in this article can be found in the appendices of [KPSW01] and [KP01], respectively. The only exception is the thermal conductivity $\kappa^{[\mathrm{SiCP}]}(T)$ of the SiC source powder, where we use the new fit

$$\kappa^{[\mathrm{SiCP}]}(T) = \left(0.00547009 \cdot \left(\frac{T}{1000\ \mathrm{K}} \right)^3 + 0.0145299 \right) \cdot \frac{\mathrm{W}}{\mathrm{mK}}. \tag{A.1}$$

As in [KPSW01, (A.6b)], $\kappa^{[\mathrm{SiCP}]}(T)$ is fitted according to curve 3 in [KRRS98, Fig. 7(a)], fixing $\kappa^{[\mathrm{SiCP}]}(1000\ \mathrm{K}) = 0.02\,\frac{\mathrm{W}}{\mathrm{mK}}$ and $\kappa^{[\mathrm{SiCP}]}(2500\ \mathrm{K}) = 0.1\,\frac{\mathrm{W}}{\mathrm{mK}}$. In the used temperature range, the dependence according to [KPSW01, (A.6b)] and according to (A.1) above is almost identical. However, in contrast to the exponential ansatz in [KPSW01, (A.6b)], the T^3-ansatz reflects the physical theory of contributions from radiative heat transfer through powder pores. Curve 3 in [KRRS98, Fig. 7(a)] corresponds to a particle diameter of 0.1 mm, a porosity of 0.45, and a pressure of 1330 Pa. All of these quantities vary in actual growth experiments. These values have been chosen for definiteness and since they reflect the qualitative behavior of most of the results in [KRRS98], where the thermal conductivity is usually an increasing function of T, having its range between $5 \cdot 10^{-3}\,\frac{\mathrm{W}}{\mathrm{m\ K}}$ and $5 \cdot 10^{-1}\,\frac{\mathrm{W}}{\mathrm{m\ K}}$.

For the numerical experiments considered in Fig. 6, the law for $\kappa^{[\mathrm{SiCP}]}(T)$ according to (A.1) has been multiplied by 3 and 5, respectively.

References

[BKP+99] N. Bubner, O. Klein, P. Philip, J. Sprekels, and K. Wilmański. *A transient model for the sublimation growth of silicon carbide single crystals*. J. Crystal Growth **205** (1999), 294–304.

[BMH+93] D.L. Barrett, J.P. McHugh, H.M. Hobgood, R.H. Hopkins, P.G. McMullin, R.C. Clarke, and W.J. Choyke. *Growth of large SiC single crystals*. J. Crystal Growth **128** (1993), 358–362.

[CTG+99] C.H. Carter, Jr., V.F. Tsvetkov, R.C. Glass, D. Henshall, M. Brady, St.G. Müller, O. Kordina, K. Irvine, J.A. Edmond, H.-S. Kong, R. Singh, S.T. Allen, and J.W Palmour. *Progress in SiC: from material growth to commercial device development*. Mater. Sci. Eng. B **61-62** (1999), 1–8.

[CZP+99] Q.-S. Chen, H. Zhang, V. Prasad, C.M. Balkas, and N.K. Yushin. *A System Model for Silicon Carbide Crystal Growth by Physical Vapor Transport Method*. 1999 National Heat Transfer Conference, NHTC99-222. ASME, 1999, pp. 1–8.

[CZP01] Q.-S. Chen, H. Zhang, and V. Prasad. *Heat transfer and kinetics of bulk growth of silicon carbide*. J. Crystal Growth **230** (2001), no. 1–2, 239–246.

[DCK+02] R.V. Drachev, D.I. Cherednichenko, I.I. Khlebnikov, M. Parker, and T.S. Sudarshan. *Graphitization of the seeding surface during the heating stage of SiC PVT bulk growth*, abstract for presentation at the European Conference on Silicon Carbide and Related Materials (ECSCRM), Linköping, Sweden, September 1 – 5, 2002.

[DNR+90] F. Dupret, P. Nicodéme, Y. Ryckmans, P. Wouters, and M.J. Crochet. *Global modelling of heat transfer in crystal growth furnaces*. Intern. J. Heat Mass Transfer **33** (1990), no. 9, 1849–1871.

[FKL01] J. Fuhrmann, Th. Koprucki, and H. Langmach. *pdelib: An open modular tool box for the numerical solution of partial differential equations. Design patterns*, in [pro01].

[GHTC97] R.C. Glass, D. Henshall, V.F. Tsvektov, and C.H. Carter, Jr. *SiC Seeded Crystal Growth*. Phys. Stat. Sol. (b) **202** (1997), 149–162.

[Har95] G.L. Harris (ed.). *Properties of Silicon Carbide*. EMIS Datareview Series, no. 13, Institution of Electrical Engineers, INSPEC, London, UK, 1995.

[KKZ+00] S.Yu. Karpov, A.V. Kulik, I.A. Zhmakin, Yu.N. Makarov, E.N. Mokhov, M.G. Ramm, M.S. Ramm, A.D. Roenkov, and Yu.A. Vodakov. *Analysis of sublimation growth of bulk SiC crystals in tantalum container*. J. Crystal Growth **211** (2000), 347–351.

[Kon95] A.O. Konstantinov. *Sublimation growth of SiC*, in [Har95], pp. 170–203.

[KP01] O. Klein and P. Philip. *Transient numerical investigation of induction heating during sublimation growth of silicon carbide single crystals*. Preprint No. 659, Weierstraß-Institut für Angewandte Analysis und Stochastik, Berlin, 2001, submitted.

[KP02] O. Klein and P. Philip. *Correct voltage distribution for axisymmetric sinusoidal modeling of induction heating with prescribed current, voltage, or power*. IEEE Trans. Mag. **38** (2002), no. 3, 1519–1523.

[KPSW01] O. Klein, P. Philip, J. Sprekels, and K. Wilmański. *Radiation- and convection-driven transient heat transfer during sublimation growth of silicon carbide single crystals*. J. Crystal Growth **222** (2001), 832–851.

[KRRS98] E.L. Kitanin, M.S. Ramm, V.V. Ris, and A.A. Schmidt. *Heat transfer through source powder in sublimation growth of SiC crystal.* Mater. Sci. Eng. B **55** (1998), 174–183.

[MGH+01] St.G. Müller, R.C. Glass, H.M. Hobgood, V.F. Tsvetkov, M. Brady, D. Henshall, D. Malta, R. Singh, J. Palmour, and C.H. Carter Jr. *Progress in the industrial production of SiC substrates for semiconductor devices.* Mater. Sci. Eng. B **80** (2001), no. 1–3, 327–331.

[PAC+99] M. Pons, M. Anikin, K. Chourou, J.M. Dedulle, R. Madar, E. Blanquet, A. Pisch, C. Bernard, P. Grosse, C. Faure, G. Basset, and Y. Grange. *State of the art in the modelling of SiC sublimation growth.* Mater. Sci. Eng. B **61-62** (1999), 18–28.

[pro01] *Proceedings of the 14th GAMM Seminar on Concepts of Numerical Software, Kiel, January 23–25, 1998.* Kiel, Germany, 2001.

[Råb96] P. Råback. *Modeling of the Sublimation Growth of Silicon Carbide Crystals.* Ph.D. thesis, Helsinki University of Technology, 1996.

[RSD+99] H.-J. Rost, D. Siche, J. Dolle, W. Eiserbeck, T. Müller, D. Schulz, G. Wagner, and J. Wollweber. *Influence of different growth parameters and related conditions on 6H-SiC crystals grown by the modified Lely method.* Mater. Sci. Eng. B **61-62** (1999), 68–72.

[SBP98] N. Schulze, D.L. Barrett, and G. Pensl. *Near-equilibrium growth of mircopipe-free 6H-SiC single crystals by physical vapor transport.* Appl. Phys. Lett. **72** (1998), no. 13, 1632–1634.

[SKM+00] M. Selder, L. Kadinski, Yu. Makarov, F. Durst, P. Wellmann, T. Straubinger, D. Hoffmann, S. Karpov, and M. Ramm. *Global numerical simulation of heat and mass transfer for SiC bulk crystal growth by PVT.* J. Crystal Growth **211** (2000), 333–338.

[SVK+00] A.S. Segal, A.N. Vorob'ev, S.Yu. Karpov, E.N. Mokhov, M.G. Ramm, M.S. Ramm, A.D. Roenkov, Yu.A. Vodakov, and Yu.N. Makarov. *Growth of silicon carbide by sublimation sandwich method in the atmosphere of inert gas.* J. Crystal Growth **208** (2000), 431–441.